# Chapter 1

# Introduction

## 1.1 Background

Terrestrial and satellite communication systems have been advancing at a rapid pace over the last decade. This enormous growth in modern wireless communications and networks has opened up a variety of new applications and has placed more technical challenges to the antenna designers. These challenges are mostly in the form of radiation performance, size and cost constraints. Antennas, the RF front-end devices of wireless communication systems, are required to deliver improved radiation performance, small size and ease of fabrication and integration. Long-distance wireless communication systems for terrestrial and space applications use high gain antennas for enhanced reliability. These antennas often provide signal gain in the range of 15-25 dB [1], [2]. As the gain available from a single antenna is limited (~5 dBi), antenna arrays are employed in long-distance point-to-point terrestrial links. Reducing the size of the individual array element is critical to reducing the overall array size and the communication system's cost. Unlike space communication applications, terrestrial communication applications rely on linearly polarized radio waves, hence use linearly polarized antennas. Thus, the polarization purity of the individual array element is essential in the functionality of the high gain linearly polarized arrays. Typically, a cross-polarization level of 21 dB or above is preferred for a linearly polarized antenna [1]–[3]. Hence, compact antennas with high gain and low cross-polarization form essential components of modern wireless communication systems. Such antennas are also applicable as high quality feeds for large reflectors and as polarization sensors.

Microstrip patch antenna (MPA) is a natural choice, due to its planar structure, low profile, light weight, low cost and flexible linear / circular polarized designs. However, the radiation efficiency of MPAs is mainly limited by the losses in both the metallic elements such as the patch and the feed system, and the dielectric substrate. For instance, in the microwave frequencies, a conventional MPA exhibits an efficiency of 82−87 % [4]. Still, owing to the low profile and the ease of fabrication, MPAs are relevant in microwave communication

applications. Just like an MPA being modeled as a "leaky metallic cavity" by the cavity model [5], a DRA can be described as a "dielectric cavity antenna" with magnetic walls that allows energy loss through radiation [6]. The DRA which is inherently free from metallic elements, exhibits very high radiation efficiency due to the lack of conduction loss, hence has been proposed as a better alternative to the prevalent MPA. The radiation efficiency of DRAs is well above 90 % in the microwave band [4]. In 1983, the first practical investigation of a cylindrical DRA fed by a coaxial probe feed was reported by S.A. Long et.al [6]. Previously, dielectric resonators (DRs) served as integral parts of microwave circuits such as oscillators, filters and amplifiers. Even though the terminologies of DR and DRA are used synonymously in the context of antennas, a DR mainly implies a non-radiating structure operating in a high-quality factor (*Q*-factor) mode, while a DRA is a radiating structure or a low *Q*-factor mode structure. When looked at the construction of a DR, it is made from a high permittivity ($\varepsilon_r >> 1$) ceramic material, having low dielectric loss ($\tan\delta \sim 0$). To use the DR as an efficient radiator, it should be placed in an open environment supported with a suitable structure such as the ground plane, and excited in the suitable electromagnetic mode (low-*Q* mode) with the proper feed mechanism. In 1984, Long's work [6], was complemented by Kajfez et.al. [7] who computed for the first time the resonant frequencies, *Q*-factors and near-field distributions of several useful modes of an isolated cylindrical DR. Isolated DR implies that the DR is not loaded by any external circuits such as the source circuit. The modal information given by [7] helped DRA researchers immensely, as it helped in the design of the suitable feed mechanism to excite the desired mode, and also to suppress an undesired mode.

## 1.2 General features of the DRA

The following features of the DRA have been reported in the literatures [8][2],

- The dimension of the DRA is of the order of $\lambda_0/(\varepsilon_r)^{0.5}$, where $\lambda_0$ is the free-space wavelength and $\varepsilon_r$ is the dielectric constant of the DR. Thus, by choosing a high value of $\varepsilon_r$ ($\varepsilon_r \approx 10$ to 40), the size of the DRA can be significantly reduced.
- Low loss feature giving high radiation efficiency (> 90 %) is attractive especially at the microwave (> 1 GHz) and millimeter wave (> 30 GHz) frequencies.

- Bandwidth of a particular DRA mode can be varied over a wide range by suitably choosing the parameters such as the $\varepsilon_r$ and the DR geometry. The bandwidth (BW) of a DRA mode is inversely proportional to the quality factor ($Q$).
- Modes of the DRA have unique internal and associated external field distributions similar to that of short electric or magnetic multipoles (monopole, dipole, quadrupole etc.) giving a variety of radiation patterns.
- Conventional microwave feed mechanisms or excitation schemes are compatible with DRAs, that also supports specialized feed designs to enhance the bandwidth, cross-polar performance, gain etc.

In the last three and a half decades, DRAs have brought immense research opportunities all over the world due to its aforesaid attractions. DRs can be fabricated into different geometries such as hemispherical, cylindrical, rectangular, triangular, trapezoidal, and even more complex ones. Cylindrical shaped dielectric resonator antenna (CDRA) is widely investigated due to its analogy to cylindrical cavity, and the well-developed theoretical foundation. The fundamental $HEM_{11\delta}$ mode of a CDRA is the most popular antenna mode, due to its lowest radiation $Q$-factor, broadside radiation pattern, moderate gain, ease of excitation, and compatibility with almost all types of feed mechanisms. The above mode can be readily excited with a coaxial feed or a microstrip feed. DRAs can be excited either in the fundamental radiating mode ($HEM_{11\delta}$ mode), the higher order mode ($HEM_{12\delta}$, $HEM_{13\delta}$ etc.) mode or a combination of the two. The last decade witnessed a growing research in the higher order mode DRAs for various uses especially for bandwidth [9] and gain enhancement [10][11].

## 1.3 DRA versus MPA – Performance Comparison

The basic circular MPA comprises of a circular metallic patch [4][12] of a certain radius, displaced from a metallic ground plane by an electrically small distance ($d << \lambda_0$). The space between the patch and the ground plane is usually filled with a dielectric substrate of dielectric constant $\varepsilon_r$. If the patch in a MPA is replaced with a DR of appropriate dimensions and $\varepsilon_r$, it becomes a DRA. However, being dielectric, the DR can be directly placed on the ground plane. The geometrical comparison between a MPA and a DRA is illustrated by the schematic representations in Fig. 1.1. Similar to the MPA, the DRA can also be treated as an open

resonator having a resonant frequency decided by the resonator dimensions and material properties of the filling medium [2]. Since the dielectric wavelength is smaller than the free-space wavelength by a factor of $\varepsilon_r^{0.5}$, both the MPA and the DRA can be made compact by choosing a high value of $\varepsilon_r$, hence both are compatible with microwave integrated circuits (MICs /MMICs).

MPA and DRA share similarity in the feeding techniques also, whether it is a coaxial probe, microstrip line, coplanar waveguide or any other feed. Considering the radiation mechanism of the MPA with respect to its fundamental mode ($TM_{11}$), it can be realized that the MPA radiates through two thin slots formed between the opposing patch edges and the ground. For a DRA, the radiation from the fundamental mode ($HEM_{11\delta}$) occurs from a much larger surface that includes the two opposing side faces and the top circular face. Thus, a DRA if properly designed can have a lower *Q*-factor, hence wider impedance bandwidth, and also a broader beam width, compared to the MPA. Even though the gain of both the DRA and the MPA are comparable, in terms of the radiation efficiency, the DRA supersedes the MPA in the case of radiation efficiency. At 4.25 GHz, and with the microstrip feed, the radiation efficiency of a DRA is 92 % while that for a MPA is only 80 % [4]. At 35 GHz, (millimeter wave), the DRA provides radiation efficiency of 95 % while a MPA provides only 78 % [12].

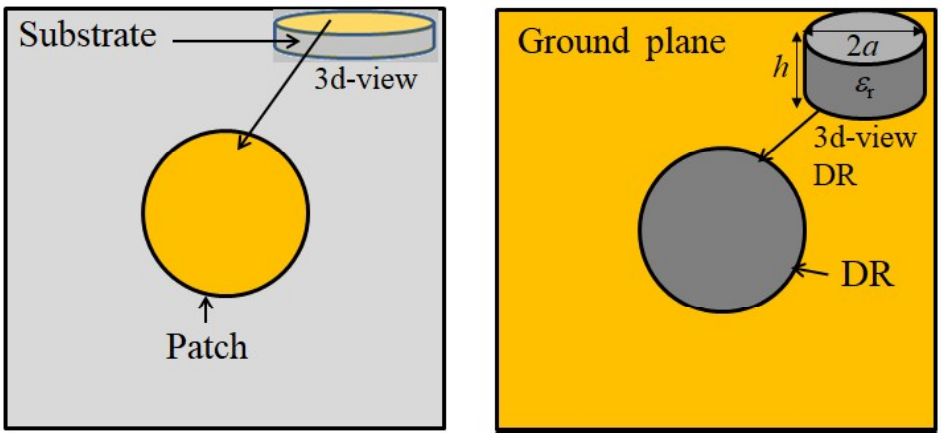


(a) (b)

Fig.1.1 Schematic representation: (a) Cylindrical microstrip patch antenna (MPA) (b) Cylindrical dielectric resonator antenna (DRA)

It should be mentioned that the performance parameters being compared between a DRA and an MPA strongly depend on the $\varepsilon_r$ and the geometry factor of the DRA / substrate respectively. MPAs are easier to fabricate using modern age printed circuit techniques. The cost of both the MPA and the DRA is decided by the cost of preparing and processing high quality microwave substrate. For example Roger's RT/Duroid [13] substrate with side = 31 cm × 46 cm, $\varepsilon_r$ = 2.33 ± 0.02 and tanδ = 0.0012 costs approximately INR 65,000. Eccostock's [14] DR cylinder of length = 31 cm, diameter = 2.5 cm, $\varepsilon_r$ = 25 and tanδ = 0.002, costs approximately INR 30,000. When the cost of substrate for making the feed is included, the DRA technology becomes much a costly affair. In terms of machinability, MPAs are much more attractive as these use thin substrates, whereas machinability has always been a major bottleneck with DRAs due to its solid and rigid structure. Even to drill a hole properly to tolerance, in a DRA for inserting a coaxial probe is a challenge. However, there are alternative feed mechanisms such as planar proximity, based feeds that are well suited with DRAs. Having said the shortcomings, DRAs are still considered suitable candidates for high frequency high efficiency applications.

## 1.4 Feed mechanisms for DRAs

The feed mechanism used to excite a certain DRA mode is designed from a knowledge of the near-field profile of that mode. The distribution of the E and the H fields inside and on the surface of the DRA gives rise to a corresponding distribution of impedance in the DRA. Now the feed point, which for most feeds is an open ended transmission line, is varied relative to the DRA, until the reflection coefficient measured at the input of the feed is minimized. At this point the DRA is said to have impedance matched to the feed / source. Once the feed point is located, the DRA is attached on the feed structure for radiation pattern measurements. A few of the feed mechanisms that are applicable to DRAs are discussed below.

### *1.4.1 Coaxial probe fed DRA*

This is probably the first type of feed proposed for DRAs. As shown in Fig. 1.2(a), the inner conductor of a coaxial connector is extended vertically through and above the ground plane where the DRA is located [6][15][16]. Impedance matching is achieved by choosing the correct probe location from the center of the DRA and the length of the probe. Probe feed has the advantages of providing a good coupling even for low permittivity DRAs, and it even avoids

the need of a matching circuit. Being in proximity with the DRA, the coaxial probe feed will also excite undesired modes, especially the higher order modes of the DRA, distorting the primary radiation pattern, especially increasing the cross-polarization. Another issue with the coaxial probe feed for low permittivity DRAs is that very often, to get good coupling, the probe needs to be protruded into the DRA. Drilling hole to precision in a DRA is a tough challenge.

### *1.4.2 Microstrip line fed DRA*

Microstrip line feed is popular as it can be fabricated by the photolithographic process, easily miniaturized and integrated with DRAs. This is probably the simplest way to excite the DRA. It being planar in nature, the DRA can be placed directly over the microstrip line to couple through proximity effect [17][18][19]. Fig. 1.2(b) shows the schematic representation of the Microstrip line fed CDRA. A metallic strip of the definite width for a given characteristic impedance is etched on one side of a thin, low permittivity substrate, the other side of which has the ground plane. Similar to the coaxial feed, the microstrip line will also excite undesired higher order modes. Additionally, the microstrip feed also suffers from surface wave loss due to the presence of the substrate to air interface.

### *1.4.3 Microstrip slot (aperture) fed DRA*

The schematic representation of the microstrip slot (aperture) fed DRA is shown in the Fig. 1.2(c). In this feed scheme, the DRA and the microstrip feed are isolated from each other by placing them on the two sides of the ground plane. Now to facilitate magnetic coupling, a thin slot is made on the ground plane directly under the DRA [20][21][11]. The impedance matching is controlled by varying the slot length and the microstrip stub length. Microstrip slot coupling is an attractive method for integrating DRAs with printed feed structures. Because of the isolation between the feed and the radiator, excitation of the higher order modes is avoided with this type of feed scheme.

### *1.4.3 Coplanar waveguide (CPW) fed DRA*

Fig. 1.2(d) illustrates the schematic diagram of the coplanar waveguide. This is made up of a thin strip separated from a pair of coplanar ground planes, and the DRA is placed on the top of this structure. Impedance matching is achieved as in the case of a microstrip line. Advantage of this technique is the high frequency response (>> 100 GHz) because connection to CPW does not involve any parasitic discontinuities in the ground plane [22][23]. However, disadvantage

of this technique is heat dissipation (depending on the thickness of the dielectric material and whether it makes contact to a heat sink). However, this feed is not as popular as the other three feeds discussed above.

### *1.4.4 Substrate integrated waveguide (SIW) fed DRA*

This is the state-of-the-art feed for millimeter wave DRAs. A model of the SIW slot fed DRA is shown in the Fig. 1.2(e). It consists of slot surrounded by the SIW (via-hole on the ground plane) and 50 Ω microstrip line is passing from the underneath of the slot. The advantages of this feeding technique are low radiation loss and high power handling capability [24]–[26]. In addition, back lobes reduce significantly compared to microstrip fed CDRA [24]. This feed is not very popular in the DRA community due to the complexity involved in the feed design and optimization.

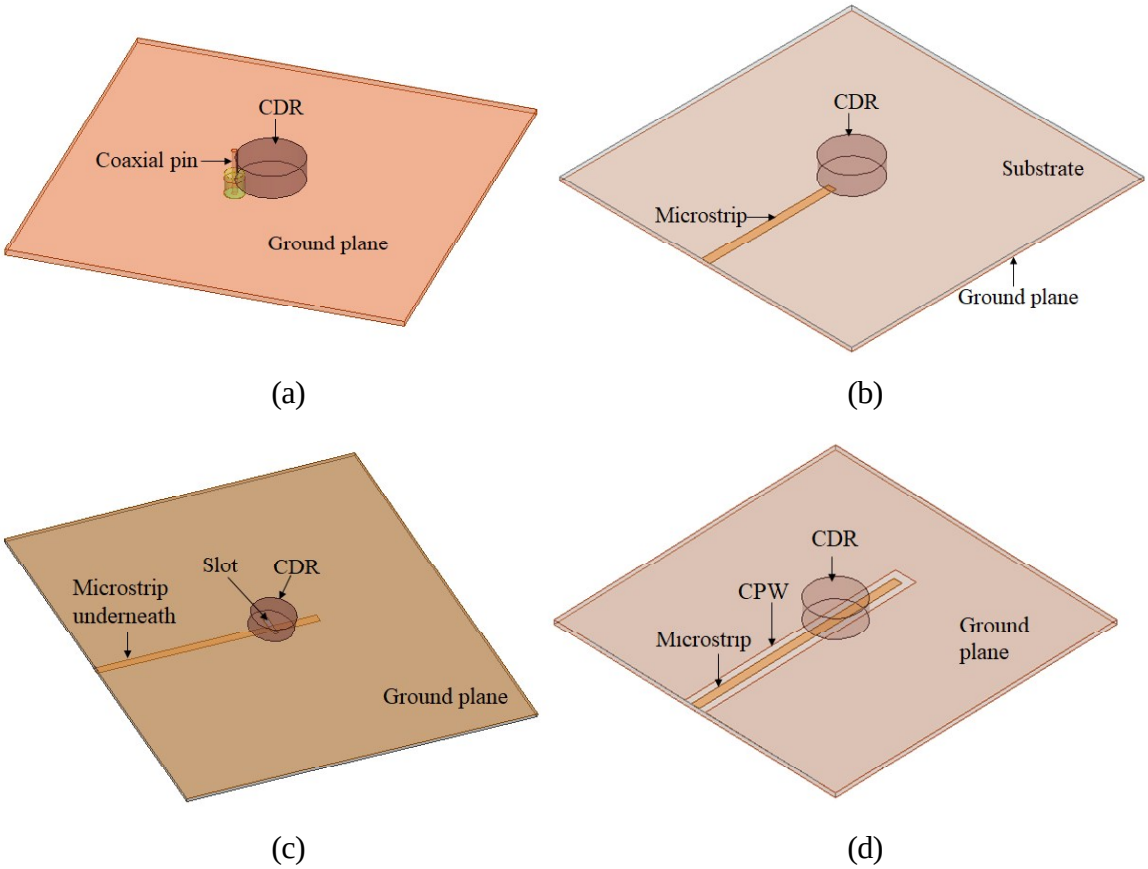

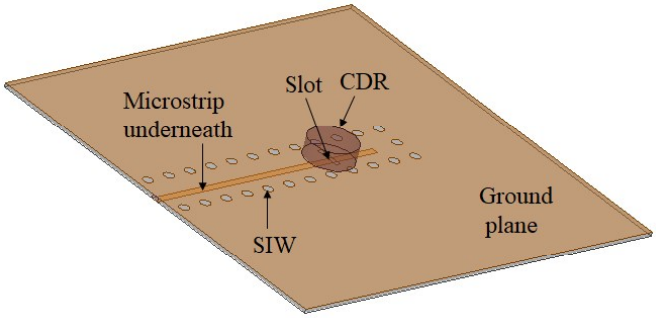


(e)

Fig. 1.2 Schematic representation of the DRA feed mechanisms (a) coaxial probe (b) microstrip line (c) microstrip slot (aperture) (d) Co-planar waveguide (e) Substrate integrated waveguide (SIW)

## 1.5 Performance characteristics of DRAs

The antenna characteristics of a DRA are attributed primarily to the electromagnetic mode which is excited in the DRA. The unique near-field distribution of the mode gives rise to a unique resonant frequency and a unique far-field pattern. These are explained below:

### *1.5.1 Electromagnetic mode and Near-field distribution*

Fig. 1.3 (a & b) shows an isolated cylindrical dielectric resonator (CDR) aligned with respect to the cylindrical coordinate specification and plane of symmetry at z = 0 respectively. As the CDR is isolated, it is free from any external loading effects, and the naturally oscillating modes are termed as the eigen modes. The eigen modes of a CDR with its axis along the z-direction, can be divided into three distinct types: TE (TE to z), TM (TM to z), and hybrid (HE and EH). The hybrid modes can be further subdivided into HE and EH modes. For HE mode, the axial electric field is comparable to the transverse electric field, whereas the axial magnetic field is negligible compared to the transverse magnetic field. All other field components for the HE modes can thus be derived from a knowledge of the $E_z$ component. The reverse is true for EH modes. With reference to the cylindrical coordinate system, to denote the variation of fields along the azimuthal, radial, and z-direction inside the resonator, the mode indices are added as subscripts to each family of modes. For example, for the $EH_{nmp+\delta}$ mode, the first index $n$ ($n$ = 0, 1, 2….) denotes the number of half-wave field variation in the azimuthal direction, with a cos $n\phi$ or sin $n\phi$ dependence.

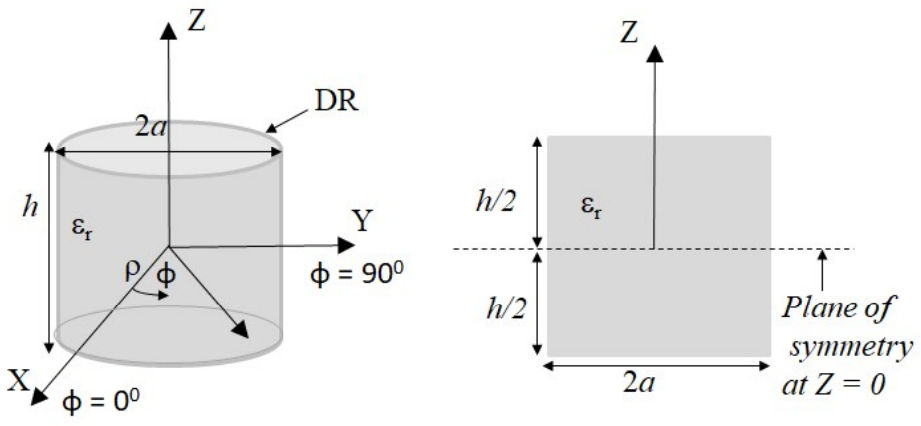


(a) (b)

Fig. 1.3 Schematic representation of the isolated CDR (a) Working coordinate specifications (b) Side view showing the plane of symmetry at Z = 0

The second index *m* (*m* = 1, 2 . . .) indicates the number of half-wave variation of the field along the radial direction. The third index *p*+δ (*p* = 0, 1, *2* . . .) where $\delta$ denotes less than half-wave variation along the axial direction (z-direction) [2], [7], [8].

For a CDR, the near-field distributions for the first five modes are shown in Fig. 1.4. The $TE_{01\delta}$ mode field distribution is similar to that of a vertical magnetic dipole, whereas the $TM_{01\delta}$ represents a vertical electric dipole shown in Fig. 1.4 (a) and (d) respectively. The $HEM_{11\delta}$ mode (Fig. 1.4 (b)) is equivalent to a magnetic dipole lying in the horizontal plane, and whereas the $HEM_{12\delta}$ (Fig. 1.4 (c)) mode closely resembles a horizontal electric dipole. The $HEM_{21\delta}$ mode of Fig. 1.4 (e) has a horizontal magnetic quadrupole nature. The E-field distribution of the $HEM_{21\delta}$ mode is not sketched as it will make the overall view unclear. The above said multi-polar nature of the modes of a DRA is responsible for distinct radiation patterns of the individual modes. An account of their resonant frequencies and *Q* values (2*a* = 10.5 mm, *h* = 4.6 mm, $\varepsilon_r$ = 38) are given in [7]. Accordingly, the $HEM_{11\delta}$ mode possesses the lowest *Q*-factor (*Q* ~ 30) and the second lowest resonant frequency, making it an ideal choice for antenna applications. This mode is called the fundamental broadside mode or the dominant broadside mode of the CDRA. The $HEM_{21\delta}$ mode exhibits the highest resonant frequency and the highest *Q*-factor (*Q* ~ 300). This high *Q* feature of the $HEM_{21\delta}$ makes it an "uninvited guest" (spurious mode) in many DRA designs.

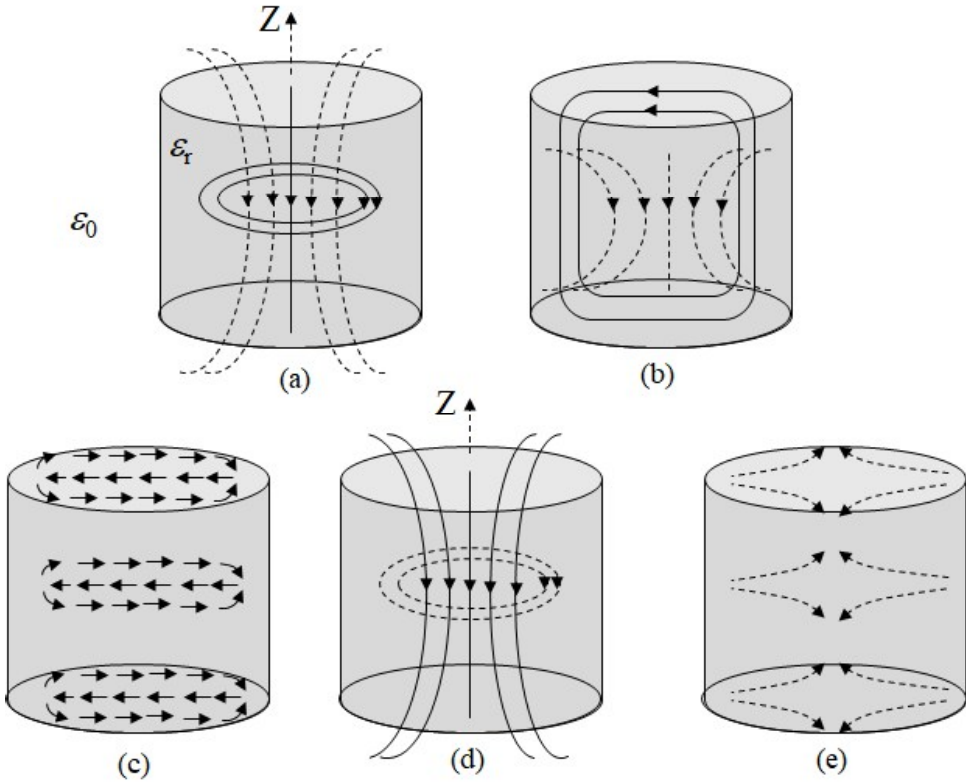


Fig. 1.4 Sketch of the near-field distribution of first five common radiating modes of the CDR (Solid lines for the E-field and broken lines for the H-field): (a) $TE_{01\delta}$ (b) $HEM_{11\delta}$ (c) $HEM_{12\delta}$ (d) $TM_{01\delta}$ (e) $HEM_{21\delta}$

#### *1.5.1.1 Resonant Frequency, Q-factor and bandwidth*

The most important attribute of a resonant mode is the resonant frequency. For a CDRA the resonant frequency of the $TE_{npm}$ or $TM_{npm}$ modes is given approximately by the magnetic wall model [6],

$$f_{npm} = \frac{1}{2\pi a\sqrt{\mu\varepsilon}}\sqrt{\left(\frac{X^2_{np}}{X'^2_{np}}\right) + \left[\frac{\pi}{2h}(2m+1)\right]^2} \qquad \ldots(1.1)$$

Where $a$ and $h$ is the radius and the height respectively of the CDRA. The constants $X_{np}$ applies for the TE modes while $X'_{np}$ for the TM modes. The above model is not practical as it assumes the DRA walls as perfect magnetic conductors i.e. $H_{tan} = 0$. This is true for very high $\varepsilon_r$ DRAs [8], but not for the DRAs of practical use.

Accurate calculation of the resonant frequency of DRAs involve solving complex integral equations using numerical methods which are very complex in nature [8]. To help the designer who is more interested in the loaded resonant frequency of the DRA mode in the presence of a particular feed mechanism, closed form equations have been proposed in different literatures [8][21]. These were obtained by using a combination of dielectric waveguide model and curve fitting technique based on extensive numerical and experimental investigations. Closed form equations for $TE_{01\delta}$, $TM_{01\delta}$, and $HEM_{11\delta}$ mode are available in the literature [8].

For a CDRA with diameter 2*a*, height *h*, aspect ratio *a/h* and dielectric constant $\varepsilon_r$, the resonant frequencies are given by [8] as,

**$TE_{01\delta}$ mode:**

$$f_{TE_{01\delta}} = \frac{2.327c}{2\pi a\sqrt{\varepsilon_r+1}}\left[1.0 + 0.2123\left(\frac{a}{h}\right) - 0.00898\left(\frac{a}{h}\right)^2\right], 0.33 \le a/h \le 5 \quad \ldots(1.2)$$

**$TM_{01\delta}$ mode:**

$$f_{TM_{01\delta}} = \frac{c}{2\pi a\sqrt{\varepsilon_r+2}}\sqrt{3.83^2 + \left(\frac{\pi a}{2h}\right)^2}, 0.33 \le a/h \le 5 \quad \ldots(1.3)$$

**$HEM_{11\delta}$ mode:**

$$f_{HEM_{11\delta}} = \frac{6.324c}{2\pi a\sqrt{\varepsilon_r+2}}\left[0.27 + 0.36\left(\frac{a}{2h}\right) - 0.02\left(\frac{a}{2h}\right)^2\right], 0.4 \le a/h \le 6 \quad \ldots(1.4)$$

Now the total quality factor ($Q_{tot}$) for a DRA may be defined as [2],

$$Q_{tot} = \frac{2\omega W_e}{P_{tot}} \quad \ldots(1.5)$$

where $W_e$ and $P_{tot}$ are the stored electrical energy (J) and the dissipated power (W), respectively, and $\omega$ is the angular frequency (rad/sec). For a DRA having negligible Ohmic losses ($tan\delta \sim 0$), the total power dissipation is dominated by the radiated power (which is also a power loss), and the total quality factor reduces to the radiation quality factor, or $P_{tot} = P_{rad}$ and $Q_{tot} = Q_{rad}$. Now the impedance bandwidth of the DRA can be estimated as,

$$BW = \frac{S-1}{Q\sqrt{S}} \quad \ldots(1.6)$$

where *S* is the maximum acceptable voltage standing-wave ratio (VSWR) defined as:

$$VSWR = \frac{1+|\Gamma|}{1-|\Gamma|} \quad \ldots(1.7)$$

Where $|\Gamma|$ is the reflection coefficient defined as:

$$|\Gamma_{in}| = \frac{Z_{in}-Z_0}{Z_{in}+Z_0} \quad \ldots(1.8)$$

Where $Z_{in}$ is the input impedance of the DRA and $Z_0$ is the characteristic impedance of the feeder line.

### *1.5.1.2 Far-field distribution or the Radiation Pattern*

The radiation pattern of a DRA is the plot of the magnitude of the far-zone field strength versus the angular position around the DRA, at a fixed distance from the DRA. Typically, the far-zone of an antenna starts at $d = 2D^2/\lambda_0$, where $D$ is the maximum overall dimension of the antenna, and $\lambda_0$ is the operating wavelength in free-space. Spherical coordinate system ($R$, $\theta$, $\phi$) is used as it is the best suited to radiation problems. A schematic diagram of a CDRA placed on a ground plane is shown in Fig. 1.5. With respect to Fig. 1.5, the radiation pattern can be defined as the electric field intensity in the far-field versus the elevation angle $\theta$ for a constant azimuth $\phi$. As discussed before, the shape of the radiation pattern depends on the particular mode of the DRA responsible for the pattern (Section 1.5.1).

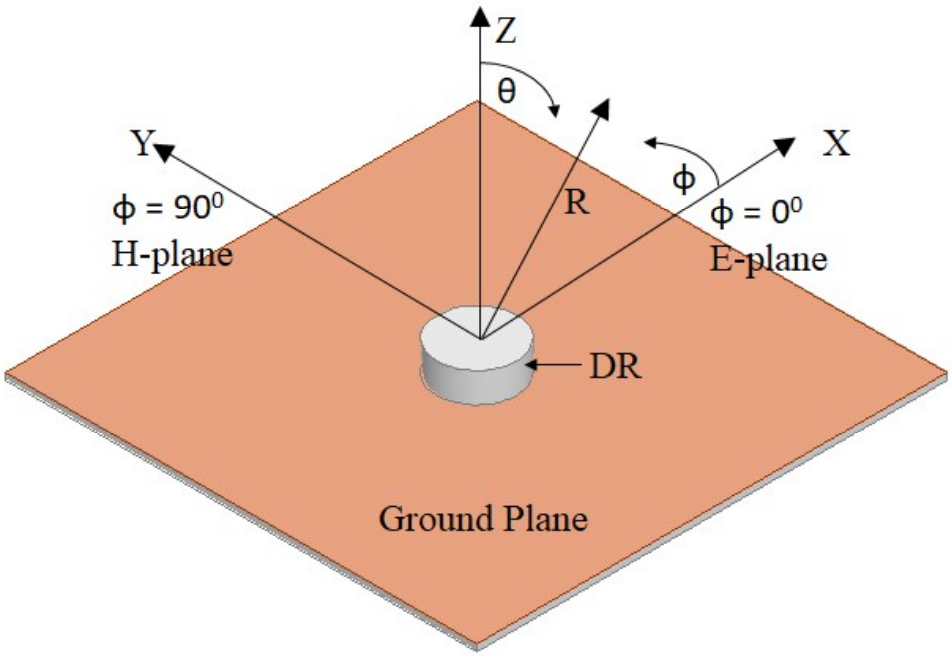


Fig. 1.5 Schematic model of a CDRA supported by finite ground plane (for arbitrary feed mechanism)

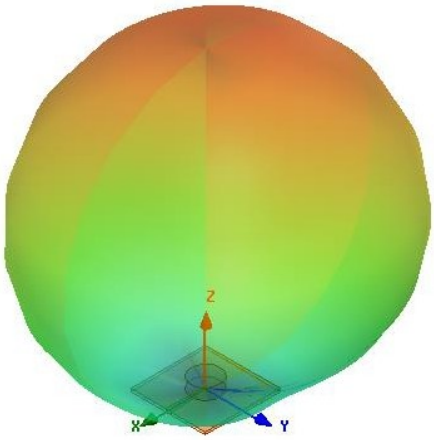


(a)

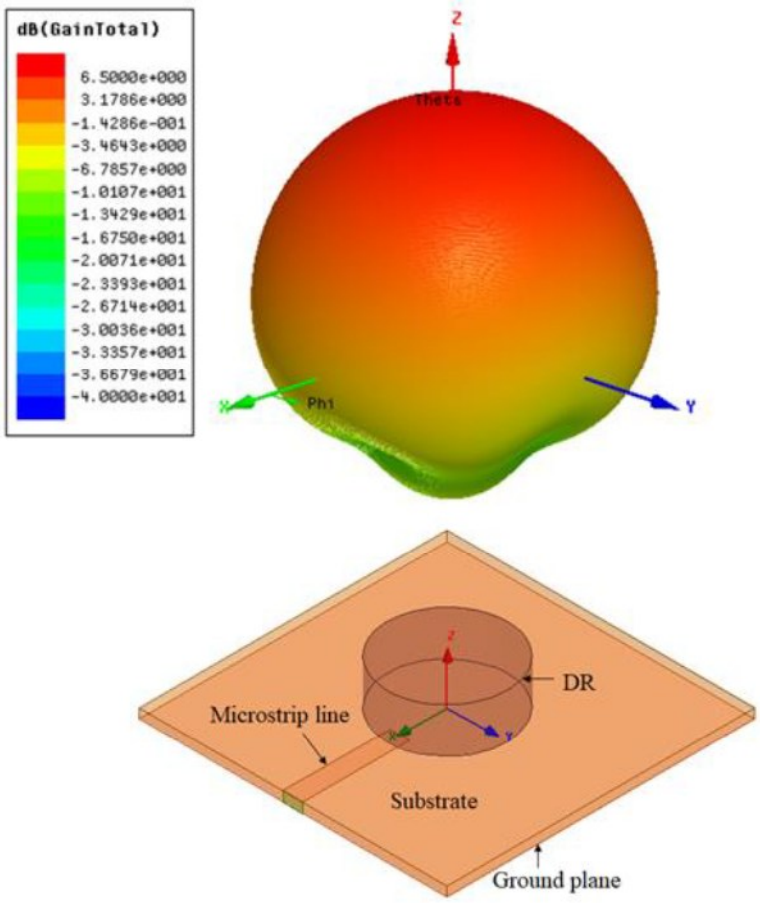


(b)

Fig. 1.6 Three-dimensional broadside radiation pattern of the $HEM_{11\delta}$ mode of the CDRA shown (a) with respect to the DRA axes (b) separately above the DRA

For example, the $HEM_{11\delta}$ mode of a CDRA radiates like a horizontal magnetic dipole, hence produces broadside radiation pattern where the maximum radiation occurs in the direction perpendicular to the ground plane or the *Z*-direction. For example, Fig. 1.6 shows the simulated 3-dimensional broadside radiation pattern of the $HEM_{11\delta}$ mode of a microstrip fed CDRA.

In this context, the polarization of the DRA can be defined as the polarization of the wave radiated by the DRA, which in turn is given by the direction of the *E*-field vector in space as a function of time. Most of the DRA designs deal with linear polarization for which the time-phase difference between the two orthogonal *E*-field components (*x* and *y* component) of the propagating wave should be 180*n* degrees, with $n = 0, 1, 2$ etc [5], that makes the *E*-field direction independent of time. Circularly polarized DRA needs stricter design where the magnitudes of the two field components should be the same, simultaneously with quadrature time-phase difference (90*n* degrees, $n = 1, 3, 5, \ldots$) between them. In linearly polarized CDRAs operated in the $HEM_{11\delta}$ mode, the feed orientation with respect to the DRA decides the unique near-field pattern, hence the polarization. Thus, the radiation characteristic of a DRA can be represented by the pair of the orthogonal polarization components i.e. the co-polarization and cross-polarization on each point of the radiation sphere. The co-polarization represents the polarization of the intended wave while cross-polarization represents the unintended wave that is orthogonally polarized. For a fairly good linearly polarized DRA, the isolation between the co-polar gain and the cross-polar gain ($G_{co} - G_{cx}$) is preferred to be > 20 dB. The cross-polar isolation when expressed as a negative number, is called the cross-polar level ($G_{cx} - G_{co}$). It has been identified that in DRAs, the $HEM_{21\delta}$ modes are responsible for the cross-polarization in the dominant $HEM_{11\delta}$ mode radiation of the CDRA [27].

With reference to Fig. 1.5, the co-polarization and the cross-polarization components of the far-field radiation can be defined by the following general relations [2].

$$E_{co} \text{ or } H_{co} = E_\theta cos\phi - E_\phi sin\phi \qquad \ldots(1.9)$$

$$E_{cx} \text{ or } H_{cx} = E_\theta sin\phi + E_\phi cos\phi \qquad \ldots(1.10)$$

From the above equations, the following table 1.1 can be generated to define the two principal plane patterns of the DRA. It can be observed that from table that $E_{co}$ and the $H_{cx}$ patterns depend on the $E_\theta$ component whereas the $H_{co}$ and the $E_{cx}$ depends on the $E_\phi$ component.

**Table 1.1 Principal planes and patterns for the DRA**

| Plane / Component | Co-polar | Cross-polar |
|---|---|---|
| E-plane ($\phi = 0^0$) | $E_{co} = E_\theta$ | $E_{cx} = E_\phi$ |
| H-plane ($\phi = 90^0$) | $H_{co} = E_\phi$ | $H_{cx} = E_\theta$ |

In addition to the cross-polar level, there are other important figures-of-merit for the DRA such as the directivity, gain and radiation efficiency that are defined as follows [5].

**The directivity (*D*)** is defined as the ratio of the maximum radiation intensity in the main beam to the average radiation intensity over all space [5]:

$$D = \frac{U_{max}}{U_{av}} = 4\pi \frac{U_{max}}{P_{rad}}. \quad \ldots(1.11)$$

$$\text{where } P_{rad} = \int_{\theta=0}^{\pi} \int_{\varphi=0}^{2\pi} U(\theta, \phi) \sin\theta d\theta d\phi \quad \ldots(1.12)$$

where $P_{rad}$ is the radiated power and $U_{max}$ is maximum the radiation intensity (W/unit solid angle). An antenna that radiates equally in all directions is called an isotropic antenna. The directivity of an isotropic element is $D = 1$ or 0 dB. Since the minimum directivity of any antenna is unity, directivity is often stated as relative to the directivity of an isotropic radiator, with unit dBi.

**The gain (*G*)** takes into account the efficiency of the antenna as well as its directional capabilities. It is defined as the ratio of the radiation intensity, in a given direction, to the radiation intensity that would be obtained if the power accepted by the antenna were radiated isotopically. The gain is given by,

$$G = 4\pi \frac{U(\theta,\phi)}{P_{in}} \quad \ldots(1.13)$$

Where $U(\theta, \phi)$ is the radiation intensity and $P_{in}$ is total input power of the antenna.

**The radiation efficiency ($\eta_{rad}$)** relates the total radiated power ($P_{rad}$) to the total input power ($P_{in}$) fed to the antenna as,

$$P_{rad} = \eta_{rad} P_{in} \quad \ldots(1.14)$$

where $\eta_{rad}$ is the antenna radiation efficiency which is contributed by conduction and dielectric losses of the DRA and the feed materials. The gain can now be expressed as,

$$G(\theta,\phi) = \eta_{rad}\left[4\pi\frac{U(\theta,\phi)}{P_{rad}}\right] \quad \ldots(1.15)$$

And the relation between the gain and the directivity is given by,

$$G(\theta,\phi) = \eta_{rad}D(\theta,\phi) \quad \ldots(1.16)$$

## 1.6 DRA modeling and Numerical predictions

With the advancements in powerful digital computer technology, and consequently computational electromagnetics, the modeling and simulation of complex antenna problems have become easier and more efficient. Commercial electromagnetic simulators – ANSYS HFSS [28] and CST Microwave Studio [29], are two commonly used by antenna designers and researchers for modeling the antenna geometry, conducting parametric analysis, optimizing the design, visualization of modal fields, and hence to make numerical predictions about the antenna.

ANSYS HFSS (High Frequency Structure Simulator) is a Finite Element Method (FEM) based 3D electromagnetic simulation software for designing and simulating high-frequency electronic products such as antennas, RF or microwave components, high-speed interconnects, filters, connectors, IC packages and printed circuit boards. Engineers worldwide use ANSYS HFSS to design high-frequency, high-speed electronics found in communications systems, radar systems, advanced driver assistance systems (ADAS), satellites, internet-of-things (IoT) products and other high-speed RF and digital devices. HFSS is basically a frequency domain solver, however it also provides eigen mode solver. Accurate results produced by HFSS simulations rely mainly on the use of tetrahedral mesh elements that fits to geometries of any complexity, and the adaptive mesh refinement that generates an accurate solution based on the physics of the design. The meshing algorithm adaptively refines the mesh throughout the geometry, it iteratively adds mesh elements in areas where a finer mesh is needed due to the localized electromagnetic field behavior.

CST Microwave Studio is a high-performance 3D EM analysis software package for designing, analyzing and optimizing electromagnetic (EM) components and systems. Common applications include the performance and efficiency of antennas and filters, electromagnetic compatibility and interference (EMC/EMI), exposure of the human body to EM fields, electro-mechanical effects in motors and generators, and thermal effects in high-power devices. CST

MWS is based on the finite integration technique (FIT), which describes Maxwell's equations on a grid space and can be written in time domain as well as in frequency domain and is not restricted to a certain grid type. Thus, MWS provides frequency domain, time domain and eigen solvers. The unique in-built feature called the perfect boundary approximation (PBA) allows the user to represent curves and inclines very accurately.

Both simulators require the following steps to be followed for simulating DRAs - (i) create the antenna geometry (ii) specify material properties (iii) assign excitations (iv) define frequency range and (v) assign radiation box. Once the solution is complete, visualizations of the results in various 1D, 2D and 3D forms can be generated, even in animated form which gives insight into the behavior of the antenna.

## 1.7 Eigen mode analysis of a CDR using HFSS

Eigen mode analysis gives an idea of the resonant frequency and the near-field pattern of several modes of an isolated CDR. This eigen mode analysis is a pre-requisite to any antenna design, as it provides the resonant frequency and field strength of the mode patterns in the source-free or the unloaded environment. This helps to design appropriate feeding mechanism to excite a certain mode while suppressing the undesired modes, or to excite multiple modes. In the following section, the HFSS eigen solver is utilized to calculate the eigenmode frequencies and near-field patterns of a CDR whose source-free resonant frequencies and near-field patterns are available in the literature [7]. This CDR has $\varepsilon_r$ = 38, $2a$ = 10.5 mm and $a/h$ = 1.1413. The simulation model is setup by locating the CDR in the middle of an air-box with perfect electric conducting (PEC) walls. The air-box has side 100 mm, so that the boundaries are sufficiently away from the near-field of the CDR modes.

The resulting HFSS model is shown in Fig. 1.7. Table 1.2 shows the computed Eigen frequencies of the five lowest modes of the CDR in comparison with [7]. It can be observed that the resonant frequencies computed in both the ways are decently matching with each other. The maximum % deviation is 2.65 % only. Although the $TE_{01\delta}$ mode has the lowest resonant frequency, it is not a preferred antenna mode due to its higher radiation quality factor compared to the $HEM_{11\delta}$ mode [7]. The electric and the magnetic field plots for the eigen modes are shown in Fig. 1.8 which are also in very good agreement with [7]. The analysis shows the fair

competency of eigen mode solver of the HFSS with the numerical model [7]. Recently in 2019, the radar cross-section (RCS) method was implemented in HFSS to compute the eigen modes of DRAs [30].

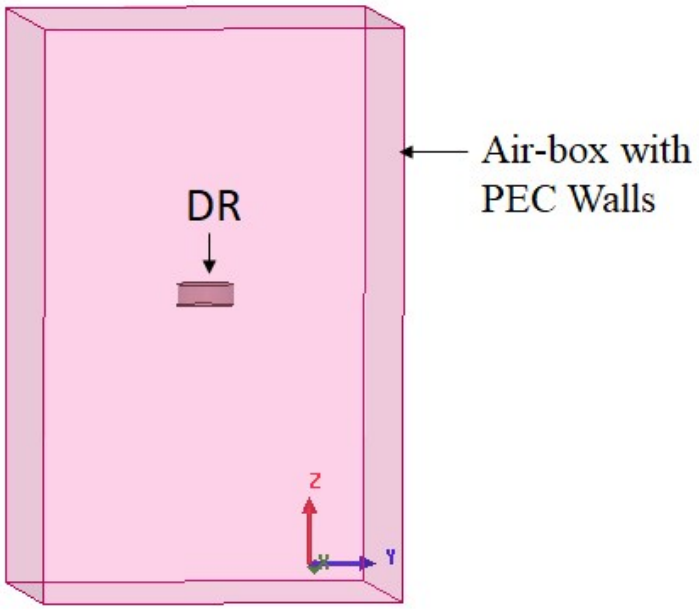


Fig. 1.7 HFSS model for eigen mode analysis of CDR ($\varepsilon_r$ = 38, 2$a$ = 10 mm, $a/h$ = 1.141)

**Table 1.2 Five lowest resonant frequency of the CDR** [7]**,** $\varepsilon_r$ **= 38, 2**$a$ **= 10.5 mm,** $a/h$ **= 1.141**

| Sl. No. | Mode | Resonant frequency $f_0$ [7] (GHz) | HFSS Eigen mode solver (GHz) | % Deviation |
|---|---|---|---|---|
| 1 | $TE_{01\delta}$ | 4.829 | 4.941 | 2.32 |
| 2 | $HEM_{11\delta}$ | 6.333 | 6.471 | 2.18 |
| 3 | $HEM_{12\delta}$ | 6.638 | 6.814 | 2.65 |
| 4 | $TM_{01\,\delta}$ | 7.524 | 7.325 | –2.65 |
| 5 | $HEM_{21\delta}$ | 7.752 | 7.813 | 0.79 |

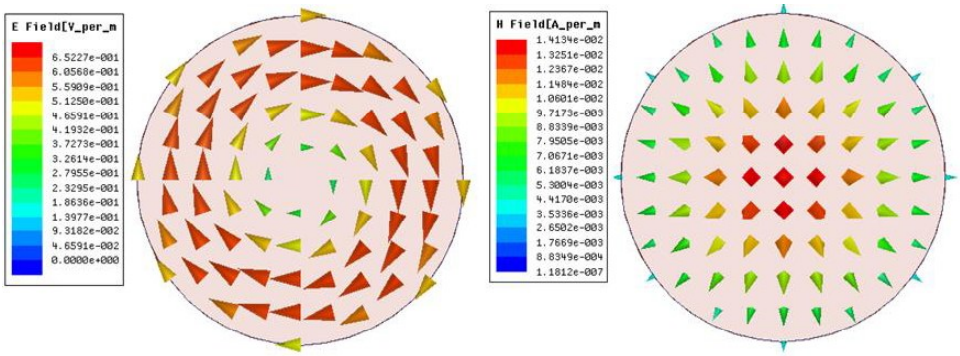


(E-field) (H-field)

(a)

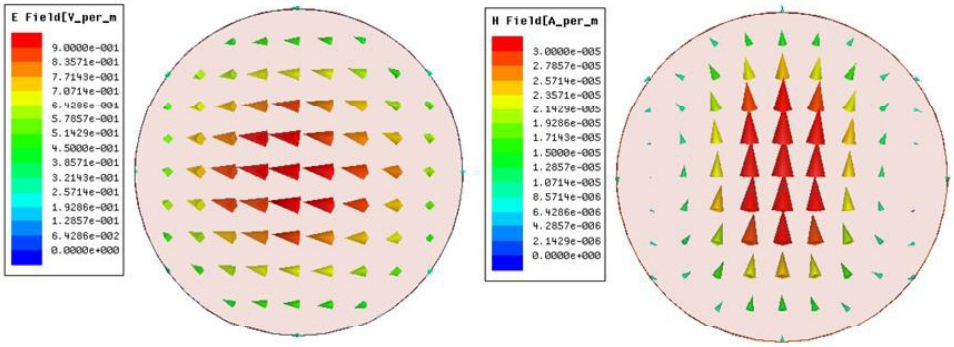


(E-field) (H-field)

(b)

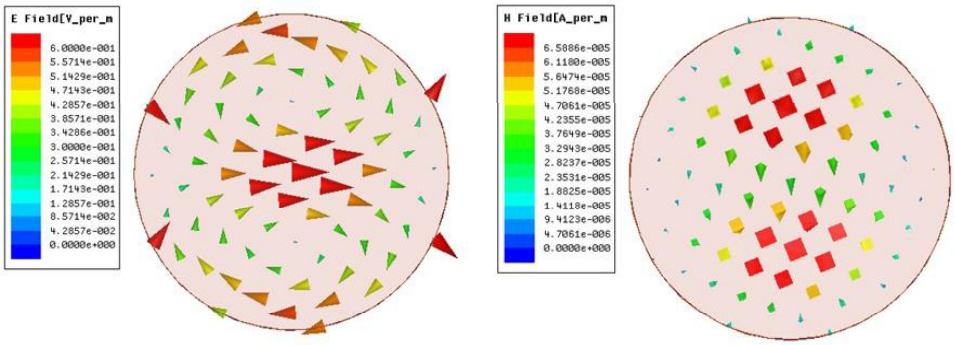


(E-field) (H-field)

(c)

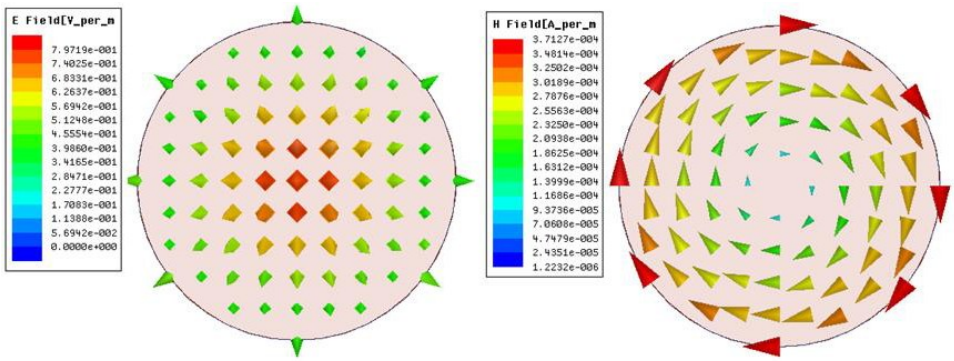


(E-field) (H-field)

(d)

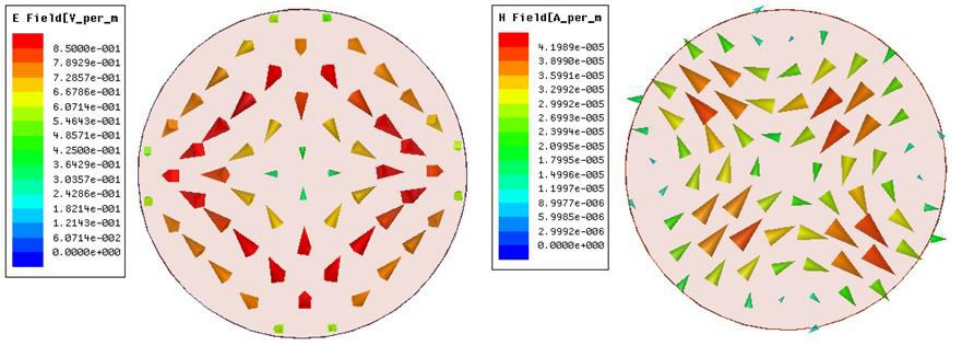


(E-field) (H-field)

(e)

Fig. 1.8 Near-field plots for the five lowest resonant frequencies of the CDRA using HFSS: (a) $TE_{01\delta}$ (b) $HEM_{11\delta}$ (c) $HEM_{12\delta}$ (d) $TM_{01\delta}$ (e) $HEM_{21\delta}$

## 1.8 Antenna Characterization

The DRA characterizations are performed with a vector network analyzer or VNA (Keysight N9928A, 30 kHz to 26.5 GHz), power meter (Agilent E4418B, –90 to + 90 dBm), power sensor (Agilent E4412A, –70 to +20 dBm), RF signal generator (Keysight N5173B, 9 kHz to 20 GHz) and a standard compact anechoic chamber. The photograph of the facility is shown in the Fig. 1.9. The VNA is used for initial frequency measurements after the prototype fabrication. Later the radiation pattern is measured by using the rest of the instruments. For this, the signal generator is connected to the transmitting antenna which is a calibrated broadband horn antenna (1 to 18 GHz). The DRA or the antenna under test is placed as the receiving antenna on a mount whose rotation can be controlled externally. The transmitter antenna is fed with 0 dBm at the

resonant frequency of the DRA, and the DRA is connected to the power meter through the power sensor to measure the received power of the antenna as a function of the spatial coordinates ($\theta, \phi$) at constant $R$ between the two antennas. Next, the gain calculation is done by using the Friis-transmission equation which for reflection and polarization-matched antennas aligned for maximum transmission is given by [5]

$$\frac{P_r}{P_t} = \left(\frac{\lambda}{4\pi R}\right)^2 G_t G_r L_t L_r \qquad \ldots(1.17)$$

Where, $P_t$ = input power of the transmitter antenna, $P_r$ = output power of the receiver antenna, $G_t$ = gain of the transmitter antenna (given by the gain vs frequency chart of the broadband horn), $G_r$ = gain of the receiver DRA (unknown), $L_t$ = cable loss on the transmitter side and $L_r$ = cable loss on the receiver side. The cable losses are separately measured through direct connection between the signal generator and the power meter.

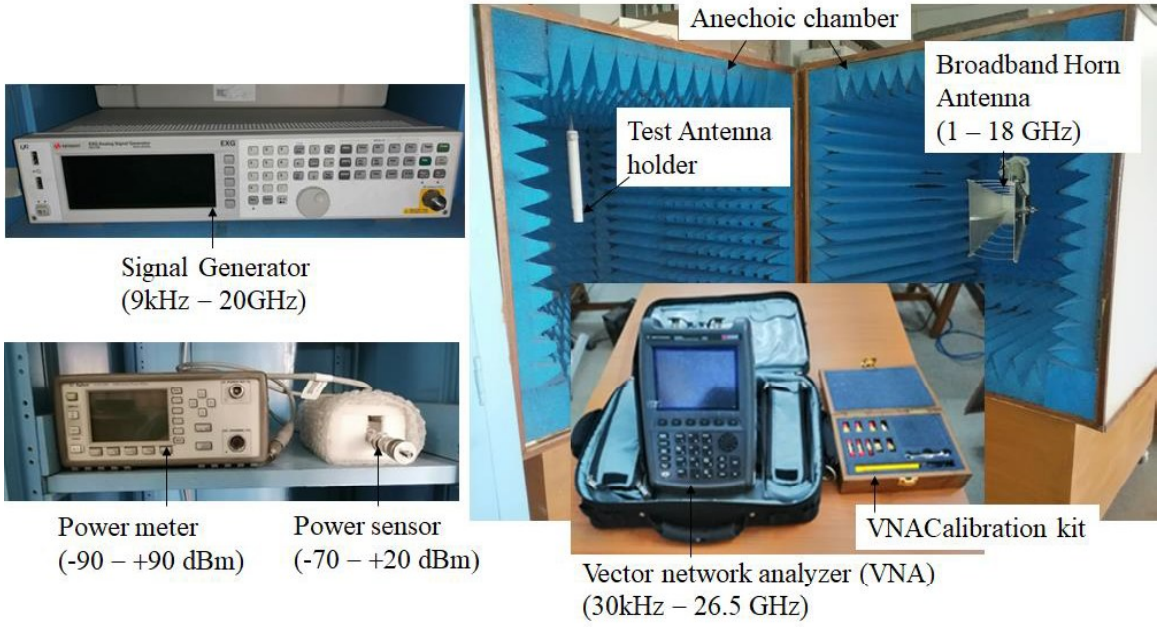


Fig. 1.9 DRA characterization facility at the parent institution

## 1.9 Motivation and Thesis Objectives

Based on the discussions made so far, a DRA can be identified as a versatile component of microwave antennas or as the antenna itself, due to its very high radiation efficiency, compact

size and capability to support a variety of radiating modes. However, the main challenges faced by compact DRA designs, are achieving (i) modal purity and (ii) high gain, without the use of complex DRA shapes or feed designs, or by incorporating additional elements to affect the compactness. Modal purity or quality refers to the absence of unwanted modes or unwanted field components pertaining to a certain higher order mode, at the operating frequency of the DRA. The presence of unwanted modal fields at the operating frequency results in (i) Distortion (asymmetry or squint) of the co-polarized radiation pattern and (ii) High cross-polarized radiation. The solution to be investigated in this thesis for achieving modal purity of the $HEM_{11\delta}$ mode of a CDRA is to suppress or detune the higher order mode(s) that are responsible for the unwanted fields at the operating frequency. The $HEM_{11\delta}$ mode being a moderate gain mode, simple techniques for improving the gain of a single DRA element are impossible. So, the method to be explored in this work is to operate the DRA at a suitable higher order mode (HOM), for which no extra complexity is required, either in the form of altered DRA shape or intricate feed geometry.

The motivation for this thesis works thus is triggered by the need for compact DRA with high gain and low cross-polarization features to be suitable for certain terrestrial communication applications. In existing literature on DRAs, there is only a handful of works that deal with the above three design goals. This motivates the author to frame the following research objectives for this thesis,

1. Study the electromagnetic properties (resonant frequency and near-field distributions) of various lower modes of a CDRA.
2. Investigate various factors such as the DRA properties (dielectric constant and dimension), feed design (feed type and ground plane dependence) etc, with respect to the excitation and the radiation pattern of various modes.
3. Compare various excitation methods in terms of frequency, gain and cross-polarization of the fundamental and the higher order modes.
4. To develop compact CDRAs for low cross-polarization and high gain.

To achieve the abovementioned objectives, the research methodology to be followed involves the literature review, DRA modelling, simulation, fabrication and experimental validation. As

discussed before (sec.1.6–1.8), commercial antenna simulation tools will be used for pre-fabrication analysis and a standard antenna measurement setup for post-fabrication validation. Comprehensive literature review needed for executing the above objectives is being presented separately in the next chapter.

## 1.10 Organization of Thesis

**Chapter 1** gave an account of the background, general features and performance characteristics of DRAs. Computer Simulation tools used for performance prediction are briefly discussed, followed by an account of the antenna simulation and characterization techniques. Later, research motivation, thesis objectives and methodology are discussed.

**Chapter 2** deals with a comprehensive review of the literature on DRAs, with emphasis placed on the low cross-polarization and higher order mode design

**Chapter 3** discusses the feed point dependence of the DRA performance, by considering three standard feed mechanisms such as the microstrip line, the microstrip slot and the coaxial probe as examples. The resonant frequency, bandwidth, radiation pattern symmetry and cross-polarized radiation levels are compared among the feeds. The feed perturbation effect is experimentally demonstrated for a microstrip fed DRA, and its near-field distribution is discussed in detail.

**Chapter 4** presents the excitation of the higher order $HEM_{21\delta}$ mode with a dual-feed network, for understanding its radiation properties. Being a low gain and axially asymmetric mode, the $HEM_{21\delta}$ mode is not a good choice for radiation. However, this mode is the major contributor to the cross-polarization in the $HEM_{11\delta}$ mode DRA. Thus, the method of metallic strip loading to suppress this mode is invented and implemented on the microstrip fed DRA to demonstrate cross-polarization reduction experimentally.

**Chapter 5** investigates an alternative yet simple design for reducing the cross-polarization of the DRA using ground size (or substrate size) optimization which has the merit of keeping the basic DRA geometry unchanged without needing any additional metallic elements as discussed in the previous chapter.

**Chapter 6** deals with the excitation of the higher order $HEM_{13\delta}$ mode of the DRA with a simple slot feed giving high gain and low cross-polarization. The resonant frequency of this particular

higher order mode is found to be related to that of the dominant $HEM_{11\delta}$ mode by a constant factor which helps in the frequency design of this mode. Later a modified feed design is presented for improving the impedance matching of the particular mode without much changing its other characteristics.

**Chapter 7** presents the thesis highlights, conclusions, and scope for future work.

## 1.11 Conclusion

In this chapter, the author presented an overview of various aspects of the dielectric resonator antenna (DRA) in a systematic fashion which lead to framing the thesis objectives. The advantages and challenges in the DRA research are briefed, in comparison with the competing MPA technology. The importance of understanding the near-field distributions of various modes of a DRA is stressed in the section on eigen mode analysis. Initial eigen modes analysis based on literatures gives the clarity of different radiating modes of CDRA. Details of various simulator tools, analysis methods and experimental techniques used are presented. Finally, the motivation, key objectives, methodology and thesis organization are briefly described.